Electronic Supplementary Information (ESI)

Surfactant-free microemulsions of 1-butyl-3-methylimidazolium hexafluorophosphate, propylamine nitrate, and water

Jie Xu,[a] Huanhuan Deng,[a] Yunlei Fu,[a] Yuquan Chen,[a] Jing Zhang,[a] Wanguo Hou *[b]

[a] *State Key Laboratory Base of Eco-chemical Engineering, Qingdao University of Science and Technology, Qingdao 266042, P.R. China;*

[b] *Key Laboratory of Colloid and Interface Chemistry (Ministry of Education), Shandong University, Jinan 250100, P.R. China*

S1. Synthesis of Propylamine Nitrate (PAN)

n-Propylamine (AR, purity ≥ 99.0%) and nitric acid (AR, 65−63% in water) used were purchased from Tianjin Chemical Reagents Co., China. PAN was prepared in our laboratory through base-acid reaction between *n*-propylamine and nitric acid, as shown in Scheme S1. Nitric acid that was prediluted to 20−25% in water was dropwise added to the equimolar quantity of *n*-propylamine at ~4 °C under magnetic stirring. The mixture was kept magnetic stirring at ~4 °C for 1 h to achieve complete reaction. Water in the crude product was removed using a rotary evaporator, and the resultant product was then dried under vacuum at 65 °C until constant weight.

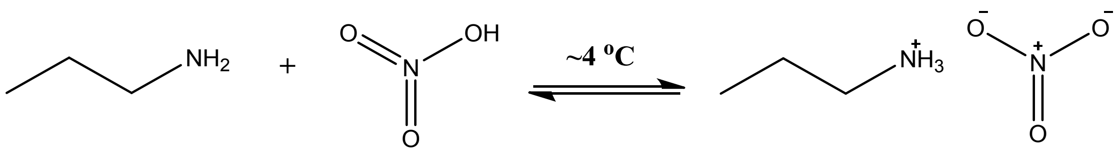

Scheme S1 Synthesis of propylamine nitrate (PAN).

(a) (b)

Fig. S1 Molecular structures of (a) $bmimPF_6$ and (b) PAN.

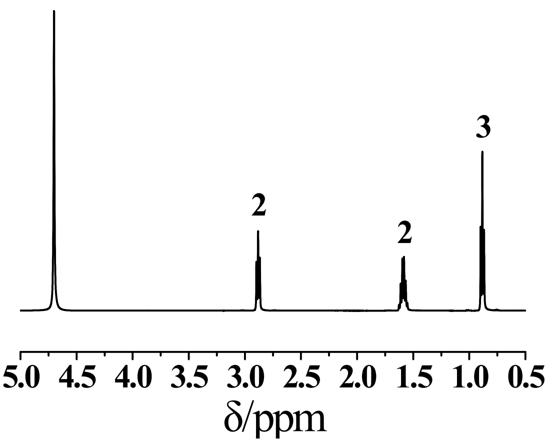

Fig. S2 ^{1}H NMR spectrum of PAN sample in D_2O.

δ 0.884 (3H, *t*, −$C\underline{H}_3$), 1.588 (2H, *m*, −$C\underline{H}_2CH_3$), and 2.882 (2H, *t*, −$C\underline{H}_2NH^{3+}$). The H in −NH^{3+} can exchange with D in D_2O, so the peak of −$N\underline{H}^{3+}$ is covered up by the characteristic peak of the solvent at 4.7 ppm. No miscellaneous peaks are observed, indicating the so-obtained PAN sample has a high purity.

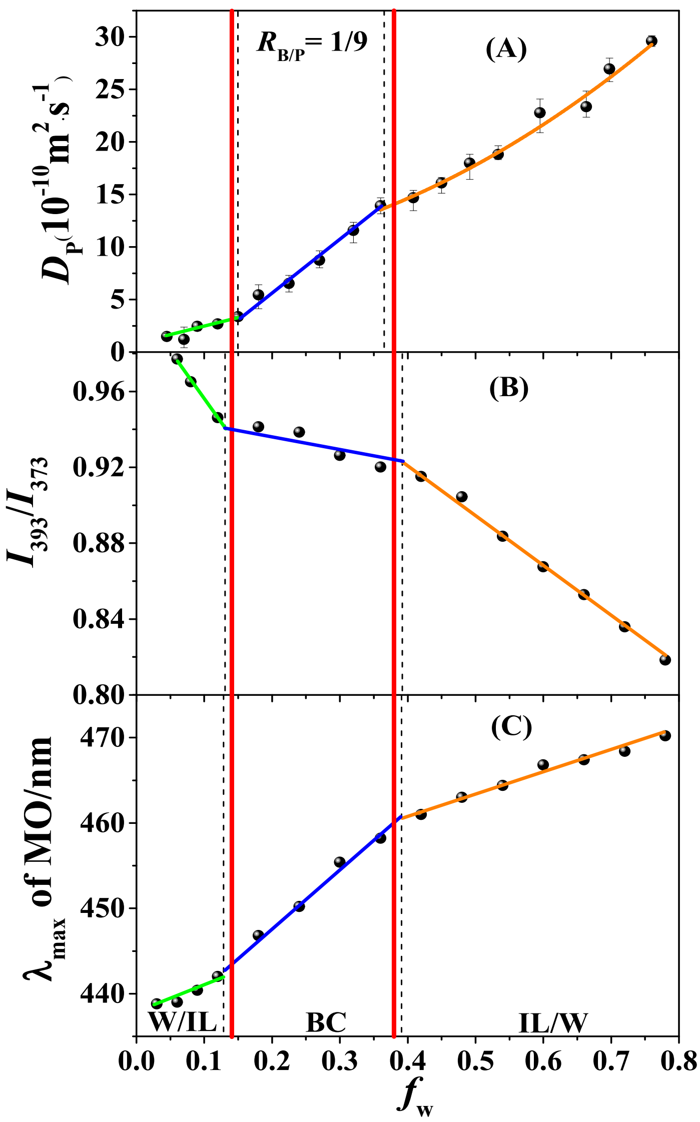

Fig. S3 (A) Diffusion coefficient (D_p) of $K_3Fe(CN)_6$, (B) intensity ratio (I_{393}/I_{373}) of pyrene, and (C) λ_{max} of MO in microemulsions at $R_{B/P}$ = 1/9 as a function of f_w. Concentrations of $K_3Fe(CN)_6$, pyrene, and MO were 0.65 g·L^{-1}, 4.95×10^{-5} mol·L^{-1}, and 0.005 g·L^{-1}, respectively.

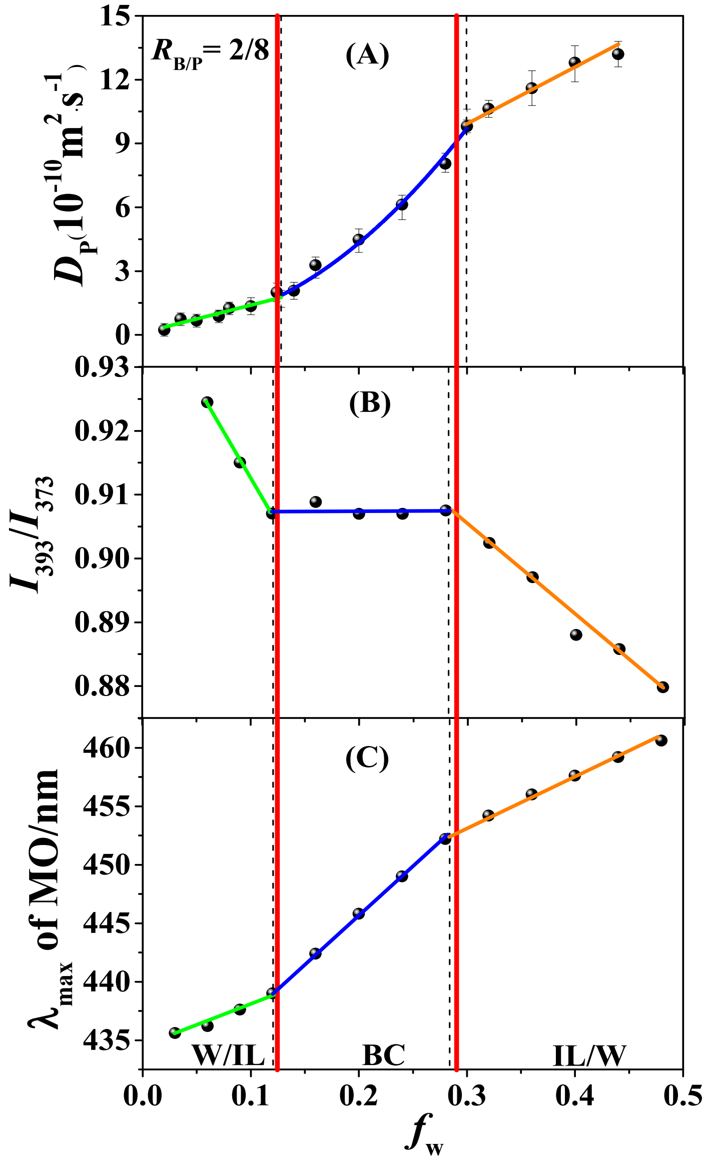

Fig. S4 (A) Diffusion coefficient (D_p) of $K_3Fe(CN)_6$, (B) intensity ratio (I_{393}/I_{373}) of pyrene, and (C) λ_{max} of MO in microemulsions at $R_{B/P}$ = 2/8 as a function of f_w. Concentrations of $K_3Fe(CN)_6$, pyrene, and MO were 0.65 g·L^{-1}, 4.95×10^{-5} mol·L^{-1}, and 0.005 g·L^{-1}, respectively.

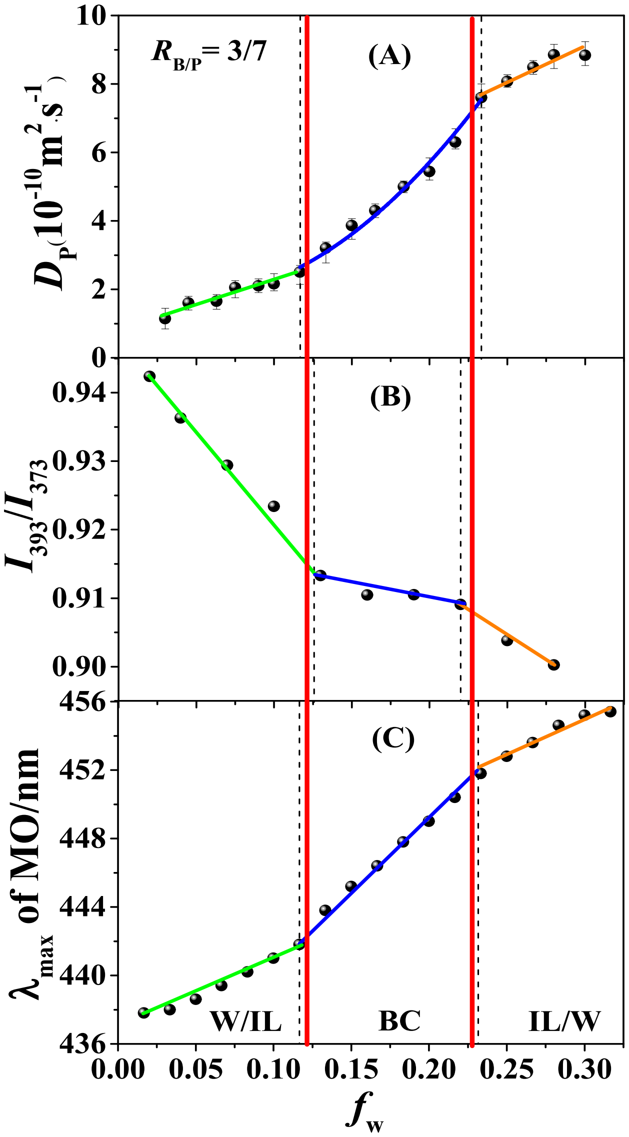

Fig. S5 (A) Diffusion coefficient (D_p) of $K_3Fe(CN)_6$, (B) intensity ratio (I_{393}/I_{373}) of pyrene, and (C) λ_{max} of MO in microemulsions at $R_{B/P}$ = 3/7 as a function of f_w. Concentrations of $K_3Fe(CN)_6$, pyrene, and MO were 0.65 $g \cdot L^{-1}$, 4.95×10^{-5} $mol \cdot L^{-1}$, and 0.005 $g \cdot L^{-1}$, respectively.

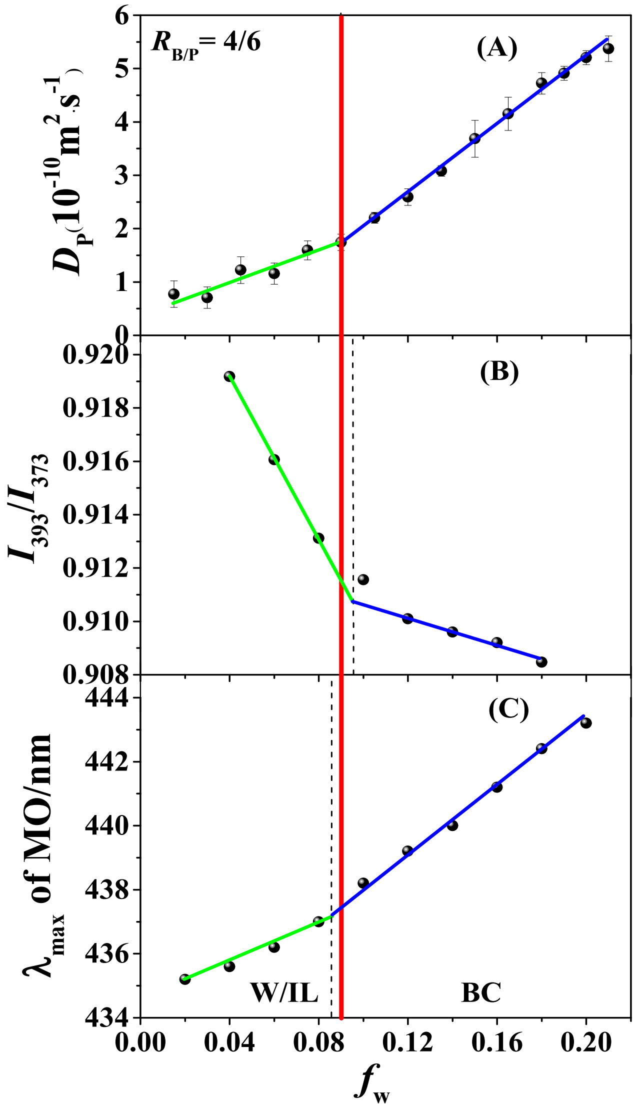

Fig. S6 (A) Diffusion coefficient (D_p) of $K_3Fe(CN)_6$, (B) intensity ratio (I_{393}/I_{373}) of pyrene, and (C) λ_{max} of MO in microemulsions at $R_{B/P}$ = 4/6 as a function of f_w. Concentrations of $K_3Fe(CN)_6$, pyrene, and MO were 0.65 g·L^{-1}, 4.95×10^{-5} mol·L^{-1}, and 0.005 g·L^{-1}, respectively.

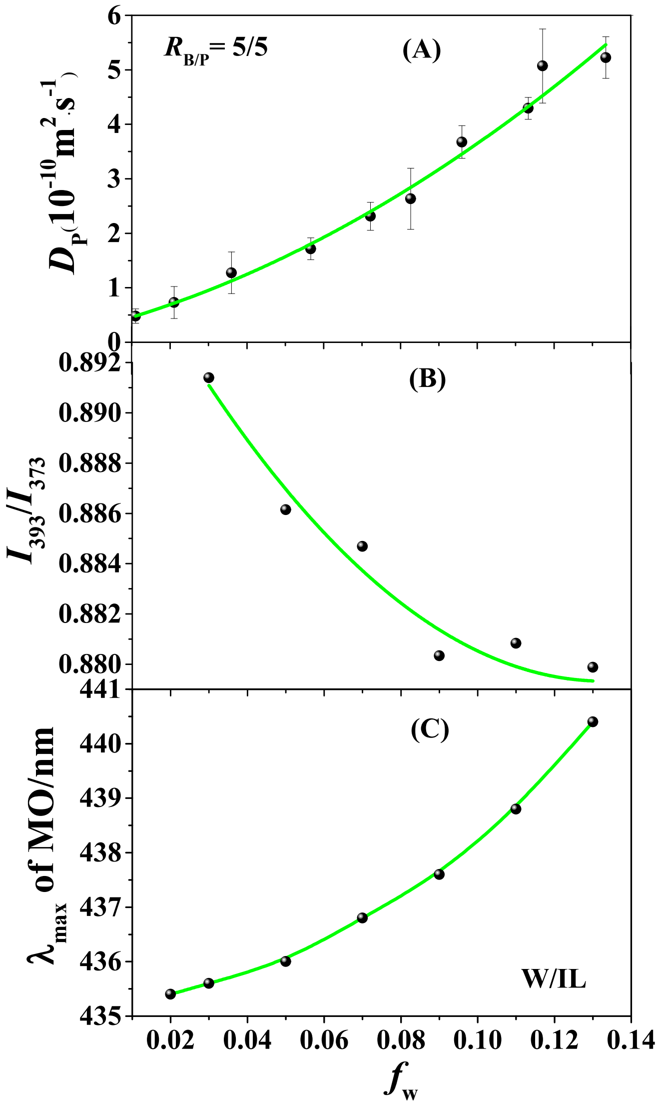

Fig. S7 (A) Diffusion coefficient (D_p) of $K_3Fe(CN)_6$, (B) intensity ratio (I_{393}/I_{373}) of pyrene, and (C) λ_{max} of MO in microemulsions at $R_{B/P}$ = 5/5 as a function of f_w. Concentrations of $K_3Fe(CN)_6$, pyrene, and MO were 0.65 g·L^{-1}, 4.95×10^{-5} mol·L^{-1}, and 0.005 g·L^{-1}, respectively.

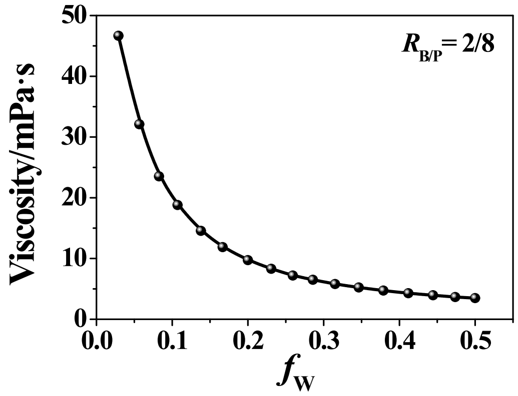

Fig. S8 Viscosity of bmimPF$_6$/PAN/water ternary system with $R_{B/P}$ = 2/8 as a function of f_W.

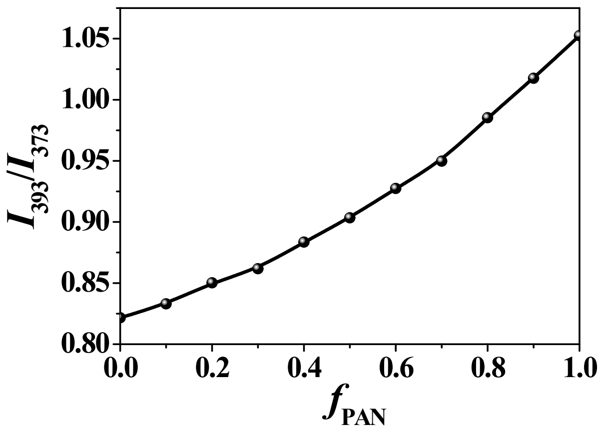

Fig. S9 Intensity ratio I_{393}/I_{373} of pyrene as a function of PAN volume fraction (f_{PAN}) in bmimPF$_6$/PAN binary solution. The pyrene concentration is 4.95×10^{-5} mol·L^{-1}.

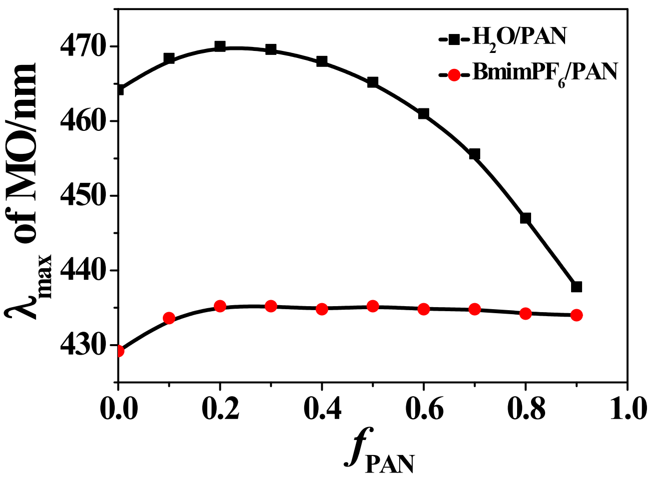

Fig. S10 MO λ_{max} as a function of f_{PAN} in $bmimPF_6$/PAN and water/PAN mixture solutions. The MO concentration is 0.005 g·L^{-1}.

Fig. S11 Photograph of $bmimPF_6$-water two-phase system containing MO. Bright orange of $bmimPF_6$ phase (low phase) indicates that MO preferentially dissolves in $bmimPF_6$ phase.

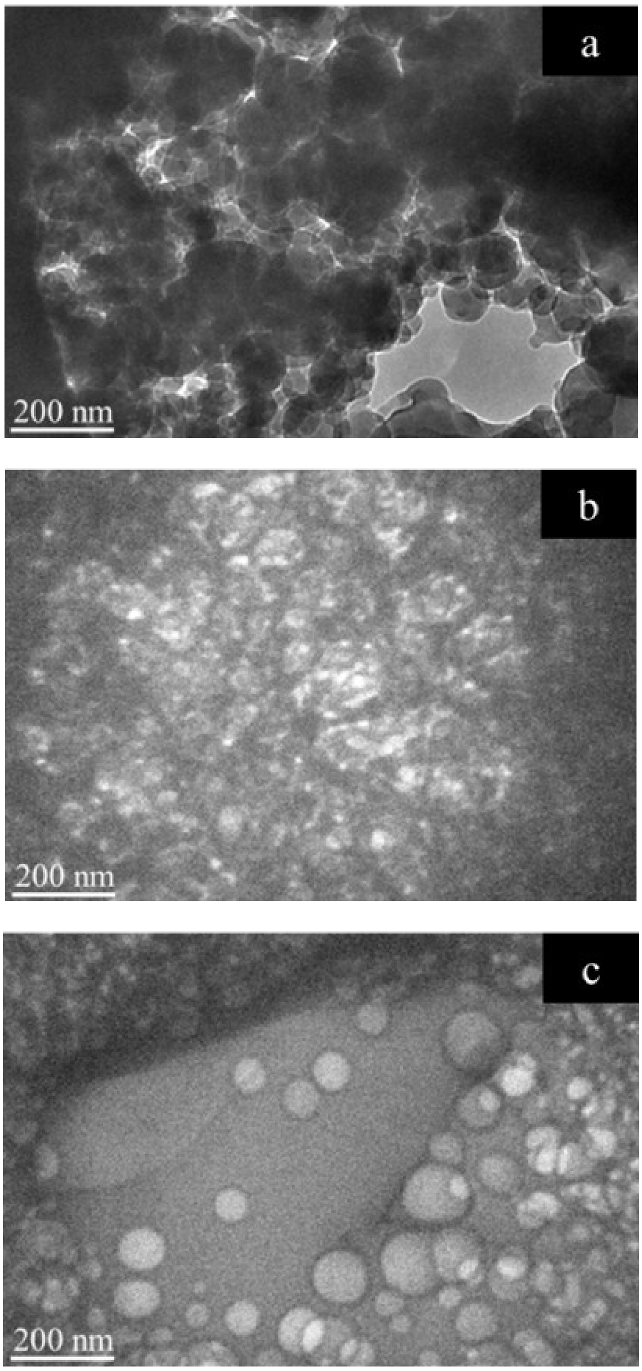

Fig. S12 Cryo-TEM images of samples with $R_{B/P/W}$ of (a) 0.286/0.667/0.047 in W/IL subregion, (b) 0.164/0.656/0.180 in BC subregion, and (c) 0.056/0.500/0.444 in IL/W subregion.

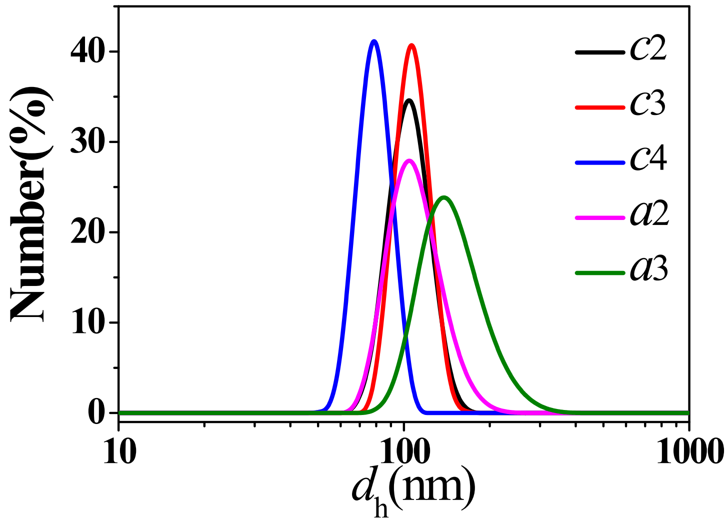

Fig. S13 Size distributions of dispersed droplets for the samples a_2, a_3, c_2, c_3, and c_4 as marked in Fig. 1.